PFG 2012 / 2, 0091 – 0104
Stuttgart, April 2012

Article

On INS/GNSS-based Time Synchronization in Photogrammetric and Remote Sensing Multi-Sensor Systems

Marta Blázquez & Ismael Colomina, Castelldefels, Spanien

Keywords: Synchronization, orientation, self-calibration, INS/GNSS, Multi-sensor systems

Summary: We propose a method to estimate time calibration parameters in the frame of a space-time integrated sensor orientation concept for the purpose of correct instrumental synchronization or synchronization verification in multi-sensor photogrammetric and remote sensing systems. The new method is based on the use of the INS/GNSS-derived velocities in addition to the commonly used INS/GNSS-derived positions and attitudes for aerial control. We present the corresponding mathematical models for local geodetic and global map-projected coordinate systems, discuss the separability between spatial and temporal calibration parameters, deduce various appropriate block configurations, and assess their behaviour with actual data. The results show that, for a number of block configurations, it is possible to correctly estimate synchronization calibration parameters with a precision of few tenths of a millisecond.

Zusammenfassung: *Über INS/GNSS-basierte Synchronisation von Multisensor-Systemen in der Photogrammetrie und Fernerkundung.* Im Beitrag wird eine Methode zur Schätzung von zeitlichen Kalibrierparametern vorgestellt, die bei Verfahren zur gemeinsamen räumlichen und zeitlichen Sensororientierung von Multisensor-Systemen eine Rolle spielen, und die entweder der richtigen Gerätesynchronisation oder deren Verifikation dienen. Der neue Ansatz berücksichtigt auch die aus den INS/GNSS-Beobachtungen abgeleitete Geschwindigkeit und nicht nur die bislang meist verwendeten Positionen und Neigungen. Der Beitrag entwickelt die mathematischen Modelle für lokale dreidimensionale kartesische und für globale projizierte Koordinatenreferenzsysteme, befasst sich mit der Trennbarkeit von räumlichen und zeitlichen Parametern, leitet daraus eine Reihe geeigneter Blockgeometrien ab und zeigt deren Verhalten mit realen Daten. Die Ergebnisse belegen, dass es bei bestimmten Blockgeometrien möglich ist, die zeitlichen Kalibrierparameter mit einer Genauigkeit von fast einer Zehntel Millisekunde zu schätzen.

1 Introduction

This paper is about the calibration of synchronization errors among the instruments of multi-sensor systems.

Synchronization errors are common in multi-sensor systems. They originate in the clocks that drive the instrumental temporal reference frames and in the delays that hardware and software introduce in the time transfer interfaces. In aerial photogrammetry and remote sensing, synchronization errors are obviously harmful in Direct Sensor Orientation (DiSO), are simply non-existent in classical aerial triangulation (Indirect Sensor Orientation, InSO), and are harmless in Integrated Sensor Orientation (ISO) because they are absorbed by the INS/GNSS per strip shifts. In the latter case they are recognizable through the usual pattern showing their flying sense dependency (Fig. 3). In terrestrial kinematic photogrammetry e.g., mobile mapping systems (Graham 2010), the various sensors are mutually and critically related by an overall system clock, usually a subsystem of an INS/GNSS-based time-Position-Velocity-Attitude (tPVA) server.

www.schweizerbart.de
DOI: 10.1127/1432-8364/2012/0104
1432-8364/12/0104 $ 3.50

Synchronization issues are usually dealt with at the hardware level by original equipment manufacturers and by system integrators. A system that is "internally well synchronized" is one in which all relevant subsystems have access to a common time reference frame within a given time error threshold. Synchronization of electrical devices and, in general, timekeeping are vast and complex engineering disciplines. Today, using off-the-shelf computer components, it is possible to design and build systems that are internally well synchronized down to 1 μs (microsecond) with a resolution of 0.1 μs. However, the resources required for correct time transfer and synchronization are not always available. Further, it is not always possible to synchronize internally well synchronized instruments to others. These situations, and possibly others, lead to what we call synchronization errors; i.e., to different time coordinates – time tags – being assigned to simultaneous events or to simply incorrect time coordinates being assigned to events. Here we assume that, contrary to the dictates of modern physics, simultaneity is an absolute concept and does not depend on the observer's reference frame.

As opposed to spatial errors, to the best of our knowledge, synchronization errors are not modelled as such and therefore can not be estimated in photogrammetric and remote sensing orientation and calibration software. Even if Integrated Sensor Orientation (ISO) can deal with them implicitly it may be better to model them explicitly. Consider, for instance, an ideal airborne ISO block consisting of n strips, affected by a constant synchronization error, with a perfectly calibrated camera and perfectly determined INS/GNSS aerial control. In this case 3 x n INS/GNSS shift unknowns could be replaced with just 1 calibration unknown; the temporal δt calibration one.

(Unfortunately, ideal blocks do not exist and there are always, small or large, original or remaining, camera calibration and INS/GNSS aerial control errors that have an influence similar to synchronization errors. As we shall see, the challenge of synchronization calibration is to distinguish between the δt calibration parameter or family of parameters from the camera calibration ones and GNSS or INS/GNSS shifts.)

The key idea behind our approach to spatio-temporal orientation and calibration is based on the observation that an INS/GNSS system delivers aerial control of the tPVA type and not just of the time-Position-Attitude (tPA) type. The use of the INS/GNSS 3D velocity estimates, in addition to those for position and attitude, makes it possible to relate time and space and consequently, allows for δt calibration in the context of spatial observations. More precisely, we will explore the combined determination of the images' orientation parameters and of the instruments' calibration parameters including the estimation of synchronization errors in an ISO block adjustment. Note that, when dealing with time, we face both orientation and calibration tasks as we have to estimate transformation parameters between different time reference frames, an orientation problem, and correction parameters – a calibration problem. Admittedly, many times, there is no essential difference between orientation and calibration.

Despite the relevance of synchronization in multi-sensor systems, in our geomatic literature research we found no discussion related to sensor synchronization calibration at the ISO or comparable levels. In robotics, where both machine vision grade and consumer grade sensors are commonly used, the synchronization problem seems to be more acute and there is a wealth of publications on the topic. However, their vast majority are unfeasible for our purposes since they require the implementation of specific communication features between the sensors like in Harrison & Newman (2011). A nice exception is the algorithm proposed in Olson (2010). However, its context is rather different from ours where we count on an INS/GNSS system and on motion. In our previous research (Blázquez & Colomina 2008) we introduced the use of INS/GNSS-derived linear and angular velocities for the estimation of constant δt in local geodetic (e, n, u) coordinate systems (l-type systems). In Blázquez (2008) actual ISO data and simulated linear velocities were combined to validate the concept. In this paper we provide detailed mathematical models for constant δt calibration with INS/GNSS-derived linear velocities in local geodetic l-type systems and in global compound mapping-geodetic (E, N, h)

coordinate systems (*m*-type systems) as well as the first analyses and validation tests with actual data. We concentrate on the determination of multi-sensor system time calibration or, in other words, time orientation between the various instruments of a multi-sensor system for the case of GNSS receivers, inertial measurement units (IMUs) and frame cameras.

The paper does not tackle the exploitation of INS/GNSS-derived rotational and angular velocities for δt determination because of the importance of properly understanding the linear velocity case. Further, the paper does not cover the case of time dependent $\delta t(t)$ synchronization errors or the similar case of internal temperature dependent or other instrumental clock $\delta t(t)$ instabilities because in many cases instrumental clocks are slaved to the few ns (nanosecond) precise output synchronization signals of GNSS receivers, thus guaranteeing stable internal time reference frames just affected by a δt time offset inaccuracy. The estimation of $\delta t(t)$ would require its modelling as a stochastic process and a dynamic observation model in the form of a stochastic differential equation or differential observation equation involving $\delta t(t)$.

Our research on time calibration in multi-sensor systems is not directly motivated by the improvement of point or orientation determination accuracy, but rather by the general progress in sensor calibration. The result of accurate time calibration is more accurate geometric calibration as geometric calibration parameters are no longer contaminated by synchronization errors. Moreover, an independent method to check the correctness of hardware instrument synchronization would be of interest to original equipment manufacturers, equipment integrators and advanced users.

The paper is organized as follows: section 2 presents the observation equations for the estimation of δt, section 3 discusses the geometry of space-time Integrated Sensor Orientation, section 4 introduces the validation criteria for the models and the overall space-time calibration concept, section 5 describes the validation data and the experiments conducted, and section 6 presents and discusses the results.

2 Mathematical Models

As mentioned, this paper introduces a new mathematical model to calibrate synchronization errors in global compound mapping-geodetic *m*-type coordinate systems and, for the sake of completeness, reviews the mathematical model in local geodetic *l*-type systems (Blázquez 2008). Both models are based on the idea presented in Blázquez (2008) "The sensor calibration and orientation problem is not a 3D spatial problem, it is a 4D spatio-temporal one. Moreover, the INS/GNSS-derived data contain not only positions and attitudes, they also contain velocities."

In *l*-type coordinate systems, the aerial control observation equations that relate the δt synchronization parameter to the position and velocity aerial observations are

$$X^l + v^l_X = P^l + R^l_c(\Gamma)\cdot(A^c + N^c) + S^l - (V^l + v^l_V)\cdot\delta t \quad (1)$$

The position control aerial equation above is complemented with the usual equation for attitude aerial control

$$R^l_c(\Gamma) = R^l_b(\chi + v_\chi)\cdot R^b_c \quad (2)$$

In *m*-type coordinate systems, the above equations become

$$X^m + v^m_X = P^m + R^m_c(\Gamma)\cdot(A^c + N^c) + S^m - M(s^m_l)\cdot R^m_l(\eta)\cdot(V^l + v^l_V)\cdot\delta t \quad (3)$$

$$R^m_c(\Gamma) = R^m_l(\eta)\cdot R^l_b(\chi + v_\chi)\cdot R^b_c \quad (4)$$

The coordinate reference frames and variables involved in (1) to (4) are described in Tabs. 1 and 2.

Tab. 1: Coordinate Reference Frames.

m	Compound mapping-geodetic global terrestrial frame (Easting-Northing-height)
l	Cartesian local terrestrial frame (east-north-up)
b	IMU instrumental frame (forward-left-up)
c	Camera instrumental frame

Tab. 2: Variables.

$X^m = (x, y, z)^m$	aerial position observation in *m*-frame
$v_X{}^m = (v_x, v_y, v_z)^m$	aerial position observation residuals in *m*-frame
$X^l = (x, y, z)^l$	aerial position observation in *l*-frame
$v_X{}^l = (v_x, v_y, v_z)^l$	aerial position observation residuals in *l*-frame
$R_b^l(\chi)$	INS/GNSS attitude matrix
$\chi_b^l = (\psi, \theta, \gamma)_b^l$	aerial attitude observation (parameterized by the traditional Euler ψ heading, θ pitch and γ roll angles)
$v_\chi = (v_\psi, v_\theta, v_\gamma)$	aerial attitude observation residuals
$V^l = (v_e, v_n, v_u)^l$	aerial velocity observation
$v_V{}^l = (v_{v_e}, v_{v_n}, v_{v_u})^l$	aerial velocity observation residuals
$P^m = (E, N, h)^m$	camera projection centre in *m*-frame
$P^l = (e, n, u)^l$	camera projection centre in *l*-frame
$R_c^m(\Gamma)$	camera attitude matrix (parameterized by the Euler angles $\Gamma_c{}^m = (\omega, \varphi, \kappa)_c{}^m$)
$R_c^l(\Gamma)$	camera attitude matrix (parameterized by the traditional Euler angles $\Gamma_c^l = (\omega, \varphi, \kappa)_c^l$)
$A^c = (a_x, a_y, a_z)^c$	camera-to-IMU lever arm
$N^c = (0, 0, n)^c$	camera nodal vector (*n* is the camera nodal distance)
$S^m = (s_E, s_N, s_h)^m$	GNSS shift correction vector in *m*-frame
$S^l = (s_e, s_n, s_u)^l$	GNSS shift correction vector in *l*-frame
δt	multi-sensor synchronization calibration parameter
R_c^b	camera-to-IMU relative attitude (boresight) matrix (parameterized by the Euler angles $\Upsilon_c^b = (v_x, v_y, v_z)_c^b$)
s_l^m	scale factor of conformal map projections that depends on P^m with $M(s_l^m) = diag(s_l^m, s_l^m, l)$
$\eta_l{}^m, R_l{}^m(\eta)$	meridian convergence angle of conformal map projections at P^m and its three-dimensional rotation matrix – rotation around the normal line to the ellipsoid through P^m – that aligns the local frame *l* to the mapping frame *m*

3 The geometry of space-time Sensor Orientation and Calibration Networks

The mathematical models introduced in the previous section together with the usual ISO models such as collinearity (photogrammetric observations), ground control (point position observations) and aerial control (tPA observations) as presented, for instance, in Blázquez & Colomina (2012) lead to a new type of photogrammetric network in which both space and time, orientation and calibration parameters are estimated. As with previously existing photogrammetric networks, like bundle self-calibrating or ISO blocks, a space-time ISO network exhibits a "geometry" that is a function of the number, quality and distribution of observations, of the models in use and of the number and distribution of unknown parameters. A "strong" geometry makes it possible to estimate more parameters than a "weak" geometry, or to better estimate them. A network's geometry is largely influenced by the block configuration; i.e. the number, distribution, length and flying sense of strips; the degree of image overlap and the ground control point distribution.

Understanding space-time network geometries makes it possible to properly configure blocks and select the models and observations required for accurate δt determination. For this purpose, we will now discuss the impact of synchronization and other related systematic errors – like camera calibration and GNSS or INS/GNSS aerial control position errors – on some relevant parameters.

A constant synchronization error Δt causes a 3D error $\Delta t \cdot V(t)$ in the aerial control position coordinates at time t and, therefore, on the ground point coordinates. In a typical aerial photogrammetric mission and within a strip, the velocity vector $V(t)$, if $V(t) = (v_E(t),v_N(t),v_h(t))^T$, is almost constant with $v_h(t) \approx 0$ and images are horizontally stabilized. Thus, the impact of the Δt error is a horizontal shift $\Delta t \cdot (v_E(t),v_N(t))^T$ where the velocity vector $(v_E(t),v_N(t))^T$ describes the instantaneous direction and sense of the trajectory. We note that the error $\Delta t \cdot (v_E(t),v_N(t))^T$ is independent from the flying height and that the size of Δt depends on the instrument and system (a 1 ms error at a flying speed of 300 km/h results in a spatial error of 8.3 cm).

It is also known that an error $(\Delta x_0,\Delta y_0)^T$ in the coordinates of the camera principal point $(x_0,y_0)^T$ results in an approximate horizontal ground shift $R_h(\kappa) \cdot m \cdot (\Delta x_0,\Delta y_0)^T$ where m is the image scale factor and $R_h(\kappa)$ is a 2D horizontal rotation of angle κ . This error is flying height-dependent and, if the camera reference frame is aligned to the forward-left-up directions of the aircraft, then the component of the error $R_h(\kappa) \cdot m \cdot (\Delta x_0,0)^T$ behaves similarly to $\Delta t \cdot (v_E(t),v_N(t))^T$.

Errors in the camera-to-IMU and IMU-to-GNSS antenna relative positions (lever arms), and even in the calibration of the GNSS receiver's antenna phase centre, have similar, flying strip sense-dependent and height-independent, effects. These errors are in the order of up to a few centimetres.

Last, the systematic errors in the GNSS or INS/GNSS aerial control observations are highly dependent on the navigation instrument quality and the observation and processing strategies. When the satellites' measurements are processed consistently, either in the differential GNSS or Precise Point Positioning (PPP) modes, the positional systematic errors are almost constant within strips or within blocks. Velocity errors can be ignored in our application because their impact is at the 10^{-5} m level. INS/GNSS systematic angular errors, contrary to what is sometimes assumed in photogrammetric modelling, are not constant due to the nature of angular velocity error propagation (triple integration) and the nature of INS/GNSS sensor fusion (errors concentrating on poor signal-to-noise ratio trajectory intervals).

Tab. 3 summarizes the identified sources of systematic errors in a space-time ISO network.

With the exception of the INS/GNSS velocities and angles, each error, e.g. Δe, discussed above can be modelled by the corresponding calibration parameter δe leading to a set of physical error models that include the parameter δe. The physical error models extend the collinearity, ground control and aerial control

Tab. 3: Main systematic error sources influencing orientation and calibration.

Error type	Scale-dependent impact	Strip sense-dependent impact	Velocity-dependent impact	Typical size	
Synchronization	no	yes	yes	< 1	ms
principal point, camera constant	yes	yes	no	1–2	px
other camera distortions	yes	-	no	**	
GNSS antenna centre	no	yes	no	1–5	cm
IMU-to-GNSS antenna	no	yes	no	0.2–2	cm
camera-to-IMU vector	no	yes	no	0.2–2	cm
camera-to-IMU rotation	yes	yes	no	0.002	deg
INS/GNSS hor. position	no	no*	no	< 5	cm
INS/GNSS ver. position	no	no*	no	<15	cm
INS/GNSS velocity	no	no*	yes	<0.01	m/s
INS/GNSS θ, γ attitude	yes	yes	no	<0.01	deg
INS/GNSS ψ attitude	yes	yes	no	<0.02	deg

*: depends on GNSS processing strategy and satellite geometry
**: depends on camera quality

ISO models with the δe's and the appropriate formulas. However, some of these calibration parameters are strongly correlated and tend to over-parameterize the estimation process leading to numerical singularities or inaccurate estimates. As is customary in these cases, simplified estimation error models, i.e. a set of observation equation models, are deduced from the complex physical error model equations. The new estimation models are adequate for the network geometries encountered in real life situations.

At this point, based on the above discussion and preliminary network adjustments, we propose a number of realistic block configurations (Tab. 4), and the corresponding calibration parameters to be estimated, or equivalently, the simplified estimation models to be used.

With the exception of configuration (a) the selected block configurations are based on typical "space ISO blocks". By "space ISO block" we understand a regular rectangular block with or without cross strips, with standard (yet camera type-dependent) forward and lateral overlaps, flown at a constant height and speed, with sparse ground control concentrated at the block ends and tPVA aerial control. The boresight matrix angles and self-calibration parameters, i.e. Ebner or Grün models, are always left as unknowns and estimated.

In all block configurations we assume correctly measured lever-arms (camera-to-IMU and IMU-to-GNSS antenna vectors), nodal vectors A^c and correctly calibrated GNSS receiver antenna phase centres.

Block configuration (a) is considered for the sake of completeness and to highlight the contribution of velocity differences to decorrelate scale-dependent and eventual INS/GNSS strip-dependent systematic errors. This configuration will not be analyzed in this paper due to a lack of actual data conforming to its requirements. Refer to Blázquez (2008) for the performance of the (a) configuration with a combination of actual and simulated data.

Block configuration (b) corresponds to the situation in which INS/GNSS positional errors are similar for the whole block and where reliable camera calibration data are available. In both (a) and (b) cases, we expect INS/GNSS positional error corrections to be separable from the δt parameter.

Block configuration (c) includes cross-strips and considers the often-encountered situation in which strips flown in different senses exhibit different velocities. While INS/

Tab. 4: Block configurations for the determination of the time calibration parameter δt.

	Block strip configuration	Block velocity configuration	Camera calibration $(\delta x_0, \delta y_0, \delta f)^c$	Time calibration δt	INS/GNSS correction $(s_E, s_N, s_h)^m$
a	alt. flying sense	velocity differences within strips	no	per system	per strip
b	alt. flying sense	approximate constant velocity in block	no	per system	per block
c	alt. flying sense and cross-strips	velocity differences among strips	only δx_0, δy_0	per system	per block
d	alt. flying sense --- 2 blocks different altitudes	approximate constant velocity within blocks	only δx_0, δy_0	per block or system	per block
e	alt. flying sense --- 2 blocks different altitudes	approximate constant velocity within blocks	yes	per block or system	1 shift for the 2 blocks

alt.: alternating

GNSS shift parameters cannot be estimated per strip, the velocity differences make it possible to separate the $(\delta x_0, \delta y_0)^{cT}$ calibration parameters from δt.

Block configurations (d) and (e) correspond to the ideal situation of two blocks for the same camera, flown at different altitudes for the purpose of decorrelating the calibration parameters that exhibit a scale-dependent impact on the parameters of interest. In this way, δt only needs to be decorrelated from the INS/GNSS shift parameters.

4 Concept Validation Criteria

A comprehensive validation of space-time ISO network calibration and orientation according to the previous network geometry discussion requires datasets that are not readily available. Fortunately (section 5), we had access to a set that, although not specifically designed for δt calibration analysis, was close enough to some of the identified Tab. 4 configurations. Given these circumstances, we will concentrate on the (b), (c), (d) and (e) block configurations since case (a) was already investigated in Blázquez (2008). Further, the validation of the space-time ISO block adjustment concept is designed as follows. Space-time ISO adjustments according to block configurations (b) to (e) will be performed. The results of the adjustment will be inspected for precision (through the standard deviations of the exterior orientation parameters (EO) and tie points (TP)), determinability (through the covariance matrices of the estimated parameters) and accuracy (by comparison to ground check point coordinates). The adjustment will be accepted if precision and accuracy are achieved and if the calibration parameters are determinable. We consider that accuracy is met if the root-mean-square error (RMSE) of the ground check points (ChP) is comparable to the RMSE of the ChPs obtained in a classical space tPA ISO adjustment. Analogously, we consider that precision is met if the mean of the standard deviations of the estimated exterior orientation (EO) and tie point (TP) parameters is similar to the classical space tPA ISO adjustment. Finally, we consider that the δt calibration parameter is well determined if there are no suspicious (according to our experience) correlations greater than 0.75 with the other estimated calibration parameters. In addition to this, with δt and $\sigma(\delta t)$ the routine significance testing can be performed.

Last, once the precision, accuracy and determinability criteria are met, a final tPA space ISO adjustment will be conducted with a free INS/GNSS shift per strip and the rest of calibration parameters fixed to the estimated values in the tPVA spatio-temporal adjustment. If the estimated INS/GNSS shifts are not stochastically significant and/or do not exhibit a strip flying sense dependency, we will declare the block well calibrated, in space and time.

5 Test Data

As mentioned, datasets to test the performance of the proposed space-time ISO method are not readily available. The Vaihingen/Enz dataset described in Kremer & Cramer (2008), although not specifically designed for the purpose, has a number of interesting features related to Tab. 4 configurations (velocity differences between strips – though moderate – and two blocks flown at different altitudes) that make it possible to derive conclusions relevant to this research. We used three blocks of the Vaihingen/Enz dataset: the Vaihingen/Enz-7 (V-7), the Vaihingen/Enz-20 (V-20) and their combination into a single two-altitude block (V-7-20). The blocks were flown in 2008, on the same day, one after the other, with IGI's Dual-DigiCAM-H/39 system and are named respectively after the nominal ground sample distance (GSD); V-7 for the 7 cm GSD block and V-20 for the 20 cm GSD

Tab. 5: Precision of observations.

Observables	V-7 & V-20 blocks
Image coordinates	$\sigma_x = \sigma_y = 1.4$ µm
Ground Control	$\sigma_E = \sigma_N = \sigma_h = 2$ cm
Aerial Control	$\sigma_E = \sigma_N = 3.5$ cm $\sigma_h = 5.5$ cm $\sigma_{ve} = \sigma_{vn} = 5$ mm/s $\sigma_{vu} = 5$ mm/s $\sigma_\gamma = \sigma_\theta = 5$ mdeg $\sigma_\psi = 8$ mdeg

one. The precision of the observations and block configurations are described in Tabs. 5 and 6 respectively. General block layouts are presented in Figs. 1 and 2.

Reference tPA space ISO adjustment results for precision and accuracy analysis are to be found in Blázquez & Colomina (2012) and Kremer & Cramer (2008). Thus, for the V-7

Tab. 6: Vaihingen/Enz-7 and Vaihingen/Enz-20 block configurations.

Test block	Vaihingen/Enz-7	Vaihingen/Enz-20
Equipment	IGI Dual-DigiCAM-H/39 Roll Angle Left H/39 -14:8 Roll Angle Right H/39 +14:8 AEROControl II-D	
Image size	2 x 5 cm x 4 cm 2 x 7216 x 5412 px	2 x 5 cm x 4 cm 2 x 7216 x 5412 px
Image size (along flight direction)	4 cm	4 cm
Image size (across flight direction)	2 x 5 cm	2 x 5 cm
Pixel size	6.8 µm	6.8 µm
Camera constant	82 mm	82 mm
Exposure time	1/800 s	1/350 s
Flying height above ground (≈)	1150 m	2750 m
Horizontal speed range (≈)	60-80 m/s	53-68 m/s
Scale (≈)	1:14000	1:33500
Ground sample distance (GSD) (≈)	10 cm	23 cm
No. of strips	6 (3+3)	3 (3+0)
No. of images	2 x 120	2 x 60
No. of images per strip (≈)	2 x 20	2 x 20
No. of photo-observations	7910 x 2	11781 x 2
No. of photo-observations per image (≈)	30 x 2	100 x 2
No. of ground control points (GCP)	8	8
No. of ground check points (ChP)	14	85
No. of tie-points (TP)	1106	2258
Overlap (≈)	60% x 76%	60% x 64%
Coordinate reference frame	m-type	m-type

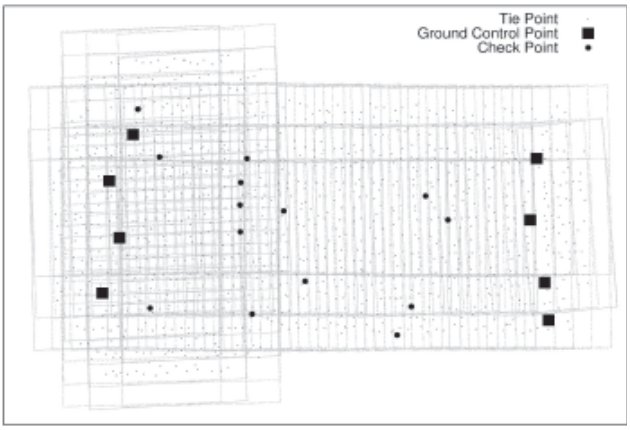

Fig. 1: Vaihingen/Enz-7 block layout.

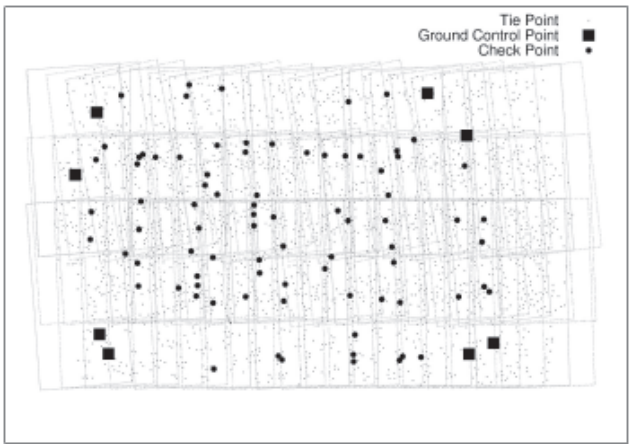

Fig. 2: Vaihingen/Enz-20 block layout.

block ChPs, accuracy (RMSE) is at the 2, 4 and 7 cm level for the two horizontal and vertical components and precision is slightly better. For the V-20 block, the RMSE of ChPs is at the 4, 7 and 17 cm level and precision is also slightly better. Precision of the images' exterior orientation parameters, also from tPA space ISO adjustments, is at the 3, 2 cm (horizontal and vertical) and 5, 3 arc sec (ω, φ and κ) level for V-7 and at the 6, 4 cm (horizontal and vertical) and 5, 3 arc sec (ω, φ and κ) level for V-20. More details on the reference precision and accuracy values are not necessary as the obtained results (section 6) are not affected by accuracy and precision problems.

Last, when dealing with synchronization of multi-head systems, there is always the question of how many δt shall be estimated: one per head or one per the combined multi-head system. In principle, both approaches are correct as long as the network geometries are strong enough and the choice is consistent with the system design. In our case, we decided to estimate one common δt for the two cameras because the dual head-system was designed for simultaneous shutter opening leaving any synchronization uncertainty as a common synchronization error (Kremer 2011).

6 Results

Tabs. 7 to 9 contain the main results of our research. All block configurations have been tested: (b) and (c) for the two blocks resulting in four test cases numbered 1 to 4; (d) and (e) for the combined V-7-20 block with a single δt parameter corresponding to test cases 5, 6 and (d) and (e) for the combined V-7-20 block with two δt parameters, for the images of the V-7 and V-20 blocks resulting in two more test cases 7, 8. For the test cases 3 to 5 and 7, the camera constants have been set and kept fixed to their nominal values; in test cases 1 and 2, the cameras' interior orientation elements have been set and kept fixed to known calibration values.

Tab. 7 describes the mean accuracy of the ground check points (ChP columns), the mean precision of the exterior orientation parameters (EO columns), the mean precision of the ground tie points (TP columns) and the precision of the camera-to-IMU [boresight] angles (Υ' column). Note that in test cases 5 to 8, the accuracy estimates are given separately for the V-7 ChPs (first row) and the V-20 ones (second row). All values are well within the acceptable ranges provided in section 5 and therefore all test cases pass the accuracy and precision validation criteria with the exception of the Northing component of the V-20 ChPs of test cases 6 and 8 (due to the global common INS/GNSS shift). As we will conclude later on, the two

cameras of the IGI Dual-DigiCAM-H/39 are already well synchronized and therefore no significant differences between the various test configurations are to be expected in the ground check point results when the δt calibration parameter is estimated.

Tab. 7 also contains the precision estimates for the camera-to-IMU, Υ_c^b, angles which are all well determined at the arc sec level and with correlations with the camera interior orientation elements of less than 0.7 and exceptionally between 0.7 and 0.8.

Tab. 8 provides bounding information on the correlation of δt with the rest of the calibration parameters. With the exception of test case 4, all test cases lead to determinable δt estimates according to the criteria set in section 4. Total correlation values $b(\delta t)$ are provided for the sake of completeness. At this point of time, the interpretation of $b(\delta t)$ is not clear; however, the $b(\delta t)$ correlations seem to indicate a stronger V-7 than V-20 geometry. This is thought to be a consequence of V-7 being a larger dataset and having cross-strips, or because of its slightly larger velocity differences.

The actual calibration results are presented in Tab. 9 where parameters significantly different from 0 are boldfaced (In Tab. 9, the standard deviation of each estimated parameter is indicated following the value of the calibrated parameter with a ± symbol.). The test case 4 will not be discussed as it did not pass the δt determinability criteria. In the table, for the test cases 3 to 8, double rows within cells of the δf, δx_0 and δy_0 columns correspond to the two cameras. Double rows within cells of the s_E, s_N and s_h columns correspond to the two INS/GNSS shifts (one per each V-7 and V-20 blocks, in the test cases 5 and 7) whereas a single row corresponds to a common shift (test cases 1 to 4, 6 and 8). A similar convention is used for the double rows within cells of the δt column for the test cases 7 and 8 where two δt calibration parameters were used (one per each V-7 and V-20 blocks).

INS/GNSS shift parameters are not significantly different from 0. This is an independent confirmation of the quality of the GNSS aerial control that, after the calibration in space and time, does not exhibit significant systematic errors.

Test cases 1, 2, 3, 7 and 8 show a remarkable consistency in the determination of a block dependent δt. If we now analyze the interior orientation elements, δf, δx_0 and δy_0, of the 3,

Tab. 7: Accuracy and precision results for the block configurations (b) to (e).

No.	Config. & Block	ChP RMSE (cm)			EO MEAN σ (cm, arc sec)					TP MEAN σ (cm)			Υ* σ (arc sec)	
		E	N	h	E_0	N_0	h_0	ω φ	κ	E	N	h	υ_x υ_y	υ_z
1	b V-7	1.9	2.4	5.7	2.2	2.1	1.8	5	3	1.5	1.8	4.1	3	2
2	b V-20	3.8	7.1	12.3	3.9	3.0	4.8	3	3	3.1	5.3	14.1	3	3
3	c V-7	1.8	2.4	5.6	2.3	2.1	1.9	5	3	1.5	1.8	4.0	3	2
4	c V-20	3.8	7.2	12.7	6.0	3.0	4.9	4	3	3.1	5.4	14.1	4	3
5	d V-7-20	2.0 3.3	2.5 6.3	6.0 11.3	2.5	2.4	2.7	4	3	2.6	4.2	10.8	2	2
6	e V-7-20	2.0 3.3	2.9 9.5	6.0 11.6	2.3	2.1	3.0	4	3	2.5	4.1	10.8	3	2
7	d V-7-20	1.9 3.4	2.5 6.2	6.0 11.1	2.9	2.4	2.7	4	3	2.6	4.2	10.7	2	2
8	e V-7-20	1.9 3.3	2.9 9.4	6.0 11.3	2.7	2.1	3.0	4	3	2.5	4.1	10.8	3	2

*: $\Upsilon_c^b = (\upsilon_x, \upsilon_y, \upsilon_z)_c^{bT}$ is the vector of boresight (camera-to-IMU) angles.

7 and 8 test cases we will see that the results of the test cases 7, 8 are consistent with each other and inconsistent with test case 3, particularly for the second camera. This may be an indication that the velocity differences between strips of the dataset used are not large enough to accurately separate δf, δx_0 and δy_0 from δt.

In principle, because of the larger number of observations and the two different block altitudes, test cases 5, 6, 7 and 8 should lead to the best results, and those most consistent among themselves. On the contrary, Tab. 9 shows that the δt and δx_0 estimates are inconsistent between the test cases 5, 6 and 7, 8. The reason for this (Kremer 2011) is the Dual-DigiCAM-H/39 time tagging convention (at the time of shutter opening) that differs from the tagging convention assumed in the paper (at the mid exposure time). According to this and to Tab. 6, a correctly synchronized Dual-DigiCAM-H/39 head with the manufacturer's convention should lead (test cases 1, 2, 3, 7 and 8) to half of 1/800 s (δt = 0.625 ms) and half of 1/350 s (δt = 1.43 ms) for the V-7 and V-20 blocks respectively. These figures are consistent with and not significantly different from the results of test cases 2, 7 and 8. They explain the differences with test cases 5, 6 and empirically confirm that block configurations (b), (d) and (e) are appropriate for tPVA space and time ISO orientation and calibration. The result is remarkable if one considers that the datasets used were not originally designed for δt calibration (A further consequence of this

Tab. 8: δt correlation bounds with the rest of calibration parameters ($\rho(\delta t, -)$) and total correlation ($b(\delta t)$).

	1	2	3	4	5	6	7	8
$\rho(\delta t, -) \leq 0.7$	yes	yes	yes	no $\rho(\delta t, \delta x_0) = 0.8$	yes	yes	yes	Yes
$b(\delta t)$	0.934	0.984	0.961	0.996	0.956	0.945	0.950 0.986	0.943 0.986

Tab. 9: Precision and determinability results for the block configurations (b) to (e).

No.	Config. & Block	Interior orientation: (μm)			INS/GNSS shifts (cm)			Time (ms)
		δf	δx_0	δy_0	s_E	s_N	s_h	δt
1	b V-7	-	-	-	-0.1 ±1.0	-2.5 ±1.0	2.7 ±1.5	-0.1 ±0.1
2	b V-20	-	-	-	0.5 ±1.8	3.5 ±2.1	-3.1 ±4.4	**1.4** ±0.4
3	c V-7	-	-2 ±1 5 ±2	**14** ±1 **-10** ±1	0.0 ±1.0	-2.5 ±1.0	4.5 ±1.5	0.0 ±0.2
*4**	*c V-20*	-	*-3 ±2* *-2 ±2*	***15*** *±2* *4 ±2*	*1.3 ±1.9*	*3.2 ±2.1*	*-3.8 ±4.5*	*0.4 ±0.8*
5	d V-7-20	-	-3 ±1 **-4** ±1	**11** ±1 -1 ±1	-0.0 ±1.0 1.6 ±1.8	-2.7 ±1.0 6.1 ±2.1	2.6 ±1.6 -0.1 ±3.9	**-0.5** ±0.1
6	e V-7-20	-2 ±2 0 ±2	**-4** ±1 -3 ±1	**12** ±1 -3 ±1	0.3 ±0.9	-1.1 ±0.9	4.1 ±2.6	**-0.5** ±0.1
7	d V-7-20	-	1 ±1 -1 ±1	**11** ±1 -1 ±1	-0.4 ±1.0 0.8 ±1.8	-2.6 ±1.0 6.1 ±2.1	2.7 ±1.6 -0.3 ±3.9	0.0 ±0.2 **1.4** ±0.4
8	e V-7-20	-2 ±2 0 ±2	0 ±1 0 ±1	**12** ±1 -3 ±1	-0.1 ±0.9	-1.0 ±0.9	4.4 ±2.6	0.0 ±0.2 **1.3** ±0.4

*: row 4 is provided just for completeness as δt did not pass the determinability criteria; it is not considered in the discussion of results.

is that block configuration (c) could be neither validated nor disregarded as the velocity differences were apparently too small.).

To conclude, as proposed in section 4, we conduct a tPA space ISO adjustment with a free INS/GNSS shift per strip and the rest of calibration parameters fixed to the estimated values in the tPVA space-time adjustment of test case 7. The results of this adjustment for the V-20 block show that the shifts are not significantly different from 0. They are depicted in Fig. 4 (All the images of the same strip have the same estimated INS/GNSS shift of the strip associated with them.). Fig. 3 shows the analogous pattern of the INS/GNSS shifts before tPVA space-time ISO orientation and calibration. As can be seen in Fig. 3, the INS/GNSS shift parameters were contaminated

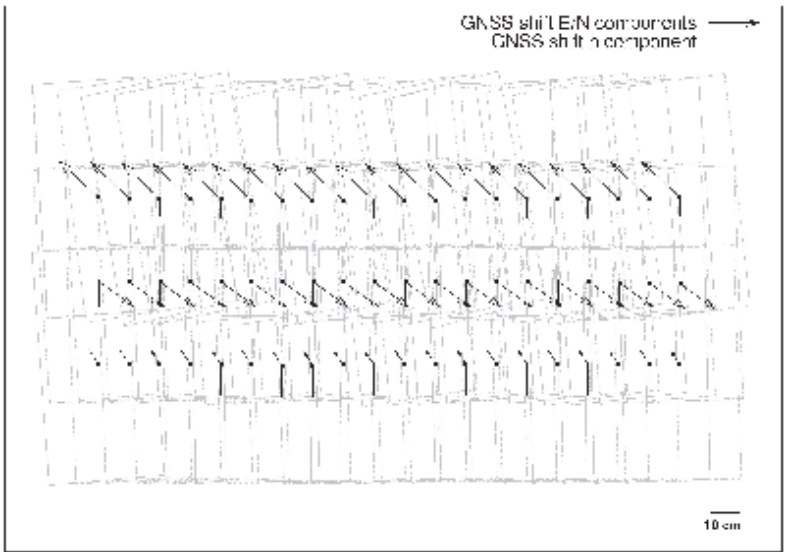

Fig. 3: V-20 INS/GNSS linear shifts before time calibration.

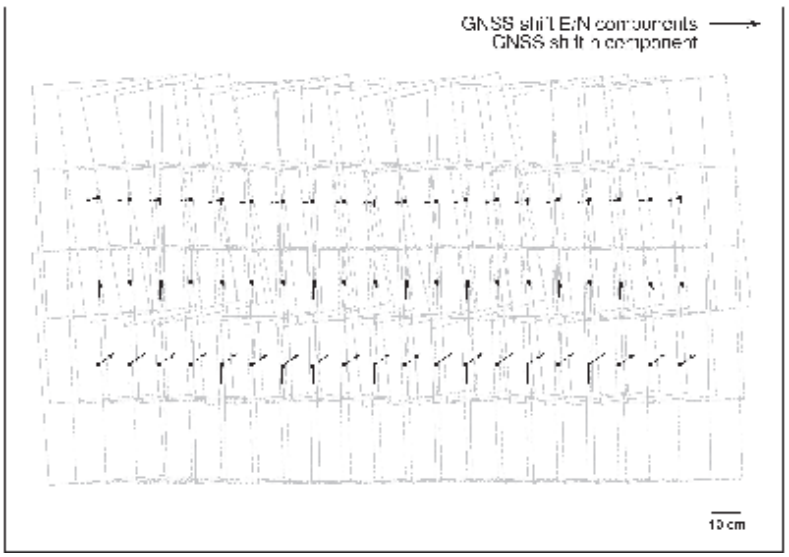

Fig. 4: V-20 INS/GNSS linear shifts after time calibration.

by flying sense-dependent spatial calibration errors. The effect of these errors vanishes in Fig. 4.

7 Conclusions

We have presented and discussed in detail the concept of spatio-temporal integrated sensor orientation for the case of constant δt synchronization calibration parameters between frame cameras and the temporal reference frame materialized by the on-board INS/GNSS system. The concept is based on the use of INS/GNSS-derived control velocities and on the decorrelation of the δt unknown parameter from other camera, system and aerial control calibration unknown parameters. Indeed, we have shown that a realistic – accurate – estimation of δt requires the careful separation between it and other calibration parameters through the appropriate block configuration. We have found that valid block configurations can be based on different altitude strips (d and e) or on standard blocks with pre-calibrated cameras (b). With the available data, we were not able to confirm that moderate velocity differences between strips (c) make it possible to separate the camera fundamental geometric calibration parameters (δf, δx_0 and δy_0) from the temporal ones δt. Cross strips are advisable because they add more data and contribute to a better determination of the camera geometric calibration parameters.

Some block configurations are more appropriate for the situation of a manufacturer's field calibration mission prior to delivery to customers; others are better suited to operational, on-the-job self-calibrating ISO. Some configurations (one INS/GNSS shift per block) are more advisable for small-area blocks and accurate short-range differential GNSS processing; others (INS/GNSS shifts per strip and velocity differences within strips) would perform better for large-area blocks and precise – though probably less accurate – long-range differential or non-differential PPP GNSS processing.

We do not claim that the mentioned and tested block configurations are the only possible ones. However, we do state that an accurate determination of δt requires separation from the camera internal geometric calibration parameters, from system calibration ones and from INS/GNSS shifts. If this is achieved by any appropriate block configuration, then the INS/GNSS-derived velocities allow for δt precisions at the tenth of a millisecond level.

We envision two main scenarios where the proposed time calibration method can be of practical interest. The first one is on the manufacturers' side for system verification and calibration purposes. In this case, the configuration of geometric test flights can be fine tuned to serve also the needs of time calibration. The second scenario is that of end users. In this case, systems that require some sort of on-the-job synchronization, high demanding specifications, the need to verify the system performance for whatever reason or pre-calibration for DiSO can benefit from our method. In the latter scenario, at least initially, we recommend a conservative approach to block configuration where scale and/or velocity differences are big. For high-end geodata acquisition systems, considering their current status and foreseen progress, system verification and calibration purposes may probably dominate its applications. For simpler systems with lower cost off-the-shelve components the method may lead to routine procedures for both verification, calibration and production purposes.

The principle of the method, using INS/GNSS-derived velocities to link space and time, can be applied to other acquisition instruments or combinations of instruments like line cameras or laser scanners. Of course, new sensing geometries may require different block configurations than those discussed in this paper.

Last, we confirm that the Dual-DigiCAM, which integrates two independent cameras, behaved as indicated by the manufacturer as what we recovered from our estimated synchronization calibration parameters was the difference between the initial (IGI convention) and mid (our convention) exposure times.

Acknowledgements

The datasets Vaihingen/Enz blocks were provided by Dr. Jens Kremer (IGI GmbH, Ger-

many) and Dr. Michael Cramer (Institut für Photogrammetrie, Universität Stuttgart, Germany). The models were implemented and the results were obtained with the Generic Extensible Network Approach (GENA) platform from GeoNumerics (Barcelona, Spain). This support for our research is greatly appreciated. The research reported in this paper has been funded by the Spanish projects LIRA (Ref. P 44/08, Ministerio de Fomento, Spain) and GeoLandModels (Ref. PET2008 071, Ministerio de Ciencia e Innovación, Spain).

References

Blázquez, M. & Colomina, I., 2008: On the Use of Inertial/GPS Velocity Control in Sensor Calibration and Orientation. – EuroSDR, ISPRS, Proceedings of the EuroCOW 2008, Castelldefels, Spain, 8 p. (on CDROM).

Blázquez, M., 2008: A New Approach to Spatio-Temporal Calibration of Multi-Sensor Systems. – International Archives of the Photogrammetry, Remote Sensing and Spatial Information Sciences **37** (B1): 481–486.

Blázquez, M. & Colomina, I., 2012: Relative INS/GNSS aerial control in integrated sensor orientation: models and performance. – ISPRS Journal of Photogrammetry and Remote Sensing **67:** 120–133.

Graham, L.I., 2010: Mobile Mapping Systems overview. – Photogrammetric Engineering and Remote Sensing **76:** 222–228.

Harrison, A. & Newman, P., 2011: TICSync: knowing when things happened. – Proceedings of the IEEE International Conference on Robotics and Automation **ICRA2011:** 356–363, Shanghai, China.

Kremer, J. & Cramer, M., 2008: Results of a performance test of a dual mid-format digital camera system. – International Archives of the Photogrammetry, Remote Sensing and Spatial Information Sciences **37** (B1): 1051–1057.

Kremer, J., 2011: Private communication.

Olson, E., 2010: A passive solution to the sensor synchronization problem. – Proceedings of the IEEE/RSJ International Conference on Intelligent Robots and Systems (IROS): 1059–1064, Taipei, Taiwan.

Address of the Authors:

Marta Blázquez, Ismael Colomina, Institute of Geomatics, Av. Carl Friedrich Gauss 11, Parc Mediterrani de la Tecnologia, E-08860 Castelldefels, Tel.: +34-93-5569280, Fax: +34-93-5569292, e-mail: {marta.blazquez}{ismael.colomina}@ideg.es

Manuskript eingereicht: Dezember 2011
Angenommen: Januar 2012